Supramolecular-Templated Synthesis of Nanoporous Zirconia−Silica Catalysts

Michael S. Wong,† Howard C. Huang, and Jackie Y. Ying*

Department of Chemical Engineering, Massachusetts Institute of Technology, Cambridge, Massachusetts 02139-4307

Received January 29, 2001. Revised Manuscript Received October 2, 2001

Thermally stable, mesoporous, and microporous zirconium-doped silica were prepared via supramolecular templating under low pH conditions. Zirconium loadings of up to 20 wt % were successfully incorporated into the porous silica-based framework, giving materials with very high surface areas, uniform pore sizes, and pore ordering. The zirconium cations were found dispersed throughout the material, and additionally, were preferentially located at the pore wall surface. The extent of Zr incorporation was found to be highly dependent on the synthesis pH and the nature of the Zr salt precursor and could be controlled by modifying the $S^+X^-I^+$ synthesis route. These Zr-doped materials showed catalytic activity for 1-butene isomerization and *cis*-cyclooctene oxidation reactions.

Introduction

There has been a great deal of research in developing supramolecular-templated mesoporous silicas for heterogeneous catalysis.[1−3] While pure mesoporous silicas, e.g., MCM-41, contain unique structural features, they are catalytically inactive, like amorphous silica gel. The general method of introducing catalytically active sites into such materials has been the chemical modification of the silica pore walls. Successful examples include the incorporation of a second metal cation into the silica-based framework;[4,5] the surface addition of metal films,[6] metal cations,[7] metal oxo species,[8] or metal oxide clusters;[9] and the surface anchoring of organometallic complexes.[10]

From a composition standpoint, mixed metal oxides have been investigated for a variety of catalytic reactions because of their enhanced acidity relative to pure metal oxides.[11] Of these materials, those composed of zirconia and silica have been found among the most strongly acidic.[12] The surface acidity comes from the difference in valence or coordination states of adjacent metal cations[11] and is affected by the relative metal amounts,[13] the molecular homogeneity of the mixed oxide,[14] and the presence of surface anions.[15] These zirconia-silicates tend to be amorphous and have low surface areas. Silicas in the form of zeolites that contain small amounts of framework Zr have generated interest as oxidation catalysts because of the importance of Ti-doped zeolites (e.g., TS-1) for commercial oxidation reactions and the similar chemistry shared by Zr and Ti.[16,17] Zirconia-silica materials with a well-defined pore structure, controllable pore sizes, and high surface areas would be advantageous for acid and oxidation catalysis.

The preparation of MCM-41 doped with a variety of metal cations has been reported by numerous research-

* To whom correspondence should be addressed.
† Present address: Department of Chemical Engineering, Rice University, Houston, TX 77251-1892.

(1) Sayari, A. *Chem. Mater.* **1996**, *8*, 1840.
(2) Corma, A. *Chem. Rev.* **1997**, *97*, 2373.
(3) Ying, J. Y.; Mehnert, C. P.; Wong, M. S. *Angew. Chem., Int. Ed. Engl.* **1999**, *38*, 56.
(4) Kresge, C. T.; Leonowicz, M. E.; Roth, W. J.; Vartuli, J. C.; Beck, J. S. *Nature* **1992**, *359*, 710. (b) Beck, J. S.; Vartuli, J. C.; Roth, W. J.; Leonowicz, M. E.; Kresge, C. T.; Schmitt, K. D.; Chu, C. T.-W.; Olsen, D. H.; Sheppard, E. W.; McCullen, S. B.; Higgins, J. B.; Schlenker, J. L. *J. Am. Chem. Soc.* **1992**, *114*, 10834. (c) Kresge, C. T.; Leonowicz, M. E.; Roth, W. J.; Vartuli, J. C. US Patent #5,098,684, 1992.
(5) For example, (a) Tanev, P. T.; Chibwe, M.; Pinnavaia, T. J. *Nature* **1994**, *368*, 321. (b) Rey, F.; Sankar, G.; Maschmeyer, T.; Thomas, J. M.; Bell, R. G.; Greaves, G. N. *Top. Catal.* **1996**, *3*, 121. (c) Tuel, A.; Gontier, S. *Chem. Mater.* **1996**, *8*, 114. (d) Zhang, L.; Ying, J. Y. *AIChE J.* **1997**, *43*, 2793.
(6) Mehnert, C. P.; Ying, J. Y. *Chem. Commun.* **1997**, 2215. (b) Mehnert, C. P.; Weaver, D. W.; Ying, J. Y. *J. Am. Chem. Soc.* **1998**, *120*, 12289.
(7) Yonemitsu, M.; Tanaka, Y.; Iwamoto, M. *Chem. Mater.* **1997**, *9*, 2679.
(8) Maschmeyer, T.; Rey, F.; Sankar, G.; Thomas, J. M. *Nature* **1995**, *378*, 159. (b) Burch, R.; Cruise, N. A.; Gleeson, D.; Tsang, S. C. *J. Mater. Chem.* **1998**, *8*, 227.
(9) Aronson, B. J.; Blanford, C. F.; Stein, A. *Chem. Mater.* **1997**, *9*, 2842. (b) Blasco, T.; Corma, A.; Martínez, A.; Martínez-Escolano, P. *J. Catal.* **1998**, *177*, 306. (c) Mulukutla, R. S.; Asakura, K.; Namba, S.; Iwasawa, Y. *Chem. Commun.* **1998**, 1425.
(10) Díaz, J. F.; Balkus, K. J., Jr.; Bedioui, F.; Kurshev, V.; Kevan, L. *Chem. Mater.* **1997**, *9*, 61. (b) Lim, M. H.; Blanford, C. F.; Stein, A. *Chem. Mater.* **1998**, *10*, 467. (c) Moller, K.; Bein, T. *Chem. Mater.* **1998**, *10*, 2950. (d) Zhang, L.; Sun, T.; Ying, J. Y. *Chem. Commun.* **1999**, 1103.
(11) Tanabe, K.; Sumiyoshi, T.; Shibata, K.; Kiyoura, T.; Kitagawa, J. *Bull. Chem. Soc. Jpn.* **1974**, *47*, 1064. (b) Tanabe, K.; Misono, M.; Ono, Y.; Hattori, H. *New Solid Acids and Bases: Their Catalytic Properties*; Kodansha: Tokyo, 1989. (c) Kung, H. H. *J. Solid State Chem.* **1984**, *52*, 191.
(12) Shibata, K.; Kiyoura, T.; Kitagawa, J.; Sumiyoshi, T.; Tanabe, K. *Bull. Chem. Soc. Jpn.* **1973**, *46*, 2985.
(13) Soled, S.; McVicker, G. B. *Catal. Today* **1992**, *14*, 189. (b) Bosman, H. J. M.; Kruissink, E. C.; van der Spoel, J.; van den Brink, F. *J. Catal.* **1994**, *148*, 660. (c) Contescu, C.; Popa, V. T.; Miller, J. B.; Ko, E. I.; Schwarz, J. A. *J. Catal.* **1995**, *157*, 244.
(14) Miller, J. B.; Rankin, S. E.; Ko, E. I. *J. Catal.* **1994**, *148*, 673. (b) Miller, J. B.; Ko, E. I. *J. Catal.* **1996**, *159*, 58.
(15) Sohn, J. R.; Jang, H. J. *J. Mol. Catal.* **1991**, *64*, 349. (b) Miller, J. B.; Ko, E. I. *Chem. Eng. J.* **1996**, *64*, 273. (c) Navío, J. A.; Colón, G.; Macías, M.; Campelo, J. M.; Romero, A. A.; Marinas, J. M. *J. Catal.* **1996**, *161*, 605.
(16) Rocha, J.; Ferreira, P.; Lin, Z.; Agger, J. R.; Anderson, M. W. *Chem. Commun.* **1998**, 1269. (b) Jale, S. R.; Ojo, A.; Fitch, F. R. *Chem. Commun.* **1999**, 411. (c) Rakshe, B.; Ramaswamy, V.; Hegde, S. G.; Vetrivel, R.; Ramaswamy, A. V. *Catal. Lett.* **1997**, *45*, 41.
(17) Notari, B. *Adv. Catal.* **1996**, *41*, 253. (b) Arends, I. W. C. E.; Sheldon, R. A.; Wallau, M.; Schuchardt, U. *Angew. Chem., Int. Ed. Engl.* **1997**, *36*, 1144.

10.1021/cm010076+ CCC: $22.00
Published on Web 04/03/2002

ers.[4,5] The doping procedure is straightforward, in which the precursor of the desired metal is added to the silicate/surfactant/water/base synthesis mixture. The metal cations are generally thought to be distributed homogeneously throughout the silicate framework, with the total amount of incorporated metal cations being low (∼2−4 wt %).[3] Higher loadings are desirable for increased catalytic activity but are difficult to achieve in doped mesoporous silicates. The highly basic solution (pH ≥ 10) required for MCM-41 synthesis appears to limit the incorporation of secondary metal cation dopants. Under such conditions, the dopant metal can separate into a second phase because of incompatible condensation and precipitation rates. Also, high levels of doping can weaken mesostructure, resulting in structural collapse after surfactant removal.[5] Careful manipulation of the templating chemistry is thus required.

The preparation of Zr-doped mesoporous silicas at high[18] and neutral[19] pH's has been studied by other researchers, although these materials were found to lose long-range pore ordering with increasing Zr loading. Still, such materials were shown to possess acidic[18,20] and oxidative properties.[19] A low-pH route to mesoporous silicas was developed by Stucky and co-workers,[21] and early work done on doped silicas via this approach had found doping levels of 1 wt %.[22]

In this article, we investigated the preparation of mesoporous Zr-doped silicas under highly acidic conditions (pH < 0). Understanding of the synthesis chemistry allowed the derivation of mesoporous silicas with as much as ∼20 wt % Zr, while maintaining pore ordering and high surface areas. The effect of Zr doping on the mesostructure was examined, and the nature of Zr in the framework was elucidated. The catalytic activity of these nanoporous materials was demonstrated for acid-catalyzed and oxidation reactions.

Experimental Section

Synthesis. A solution of zirconium sulfate tetrahydrate was prepared by dissolving a desired amount of the salt ($Zr(SO_4)_2 \cdot 4H_2O$, 99.99+%, Strem) in 15 mL of deionized water. This was combined with a solution containing cetyltrimethylammonium bromide (CTAB, 99+%, Alfa Aesar) and hydrochloric acid (37%, Mallinckrodt). Tetraethyl orthosilicate (TEOS, 98%, Aldrich) was immediately added to the mixture. The molar ratio of this precursor mixture was 10 TEOS: *x* $Zr(SO_4)_2$: 1.3 CTAB: *y* HCl: 1690 H_2O. Samples prepared with $y = 54$ (at a calculated pH of −0.25) were labeled ZrSi1-*x*, and samples prepared with $y = 5.4$ (at a higher pH of 0.75) were labeled ZrSi2-*x* (Table 1). Zirconyl chloride octahydrate ($ZrOCl_2 \cdot 8H_2O$, 98%, Aldrich) was used as an alternative Zr precursor, resulting in a sample labeled ZrSi1-3C. These samples were collectively named ZrSi. The mixture was stirred for 2 h and then aged at room temperature for 2 days. The resulting white powder was filtered and washed 3 times with water, and left to air-dry overnight. For surfactant removal, the mesostructured ZrSi samples were calcined at 540 °C for 3 h under flowing air, with a ramp rate of ∼3 °C/min. A pure mesoporous silica labeled ZrSi1-0 was prepared without addition of any Zr precursors. Pure silica ZrSi2-0 was also prepared without addition of any Zr precursors, but an aging period of two weeks was required for precipitation of a product.

Table 1. Synthesis Conditions and Elemental Analysis Results of ZrSi Materials

sample	precursor Zr/Si molar ratio	precursor HCl/Si molar ratio	calculated pH[d]	measured Zr content (wt %)[e]	expected Zr content (wt %)[e,f]
ZrSi1-0	0.0	5.4	−0.25	0.0	0.0
ZrSi1-0.2	0.02	5.4	−0.25	1.0	2.9
ZrSi1-1	0.1	5.4	−0.25	2.0	12.6
ZrSi1-3	0.3	5.4	−0.25	2.8	28.2
ZrSi1-10	1.0	5.4	−0.25	4.4	49.8
ZrSi2-0[a]	0.0	0.54	0.75	0.0	0.0
ZrSi2-0.1	0.01	0.54	0.75	1.3	1.5
ZrSi2-0.2	0.02	0.54	0.75	2.9	2.9
ZrSi2-0.4	0.04	0.54	0.75	6.1	5.6
ZrSi2-1	0.1	0.54	0.75	10.7	12.6
ZrSi2-3	0.3	0.54	0.75	16.2	28.2
ZrSi2-10	1.0	0.54	0.75	19.6	49.8
ZrSi1-3C[b]	0.3	5.4	−0.25	4.5	28.2
ZrSBA-15[b,c]	1.0	5.7	−0.30	4.8	49.8

[a] Nonmesostructured after calcination. [b] Zr precursor: $ZrOCl_2 \cdot 8H_2O$. [c] Templating surfactant: P123 triblock copolymer. [d] Based on HCl concentration. [e] Zr content after surfactant removal. [f] Based on 100% recovery of precursor used.

ZrSi with larger mesopores was prepared by using a much larger surfactant than CTAB. An acidic solution of the surfactant P123 [(ethylene oxide)$_{20}$(propylene oxide)$_{70}$(ethylene oxide)$_{20}$, FW = 5880, BASF][23] was combined with a 30 wt % solution of zirconyl chloride octahydrate. After TEOS was added, the synthesis mixture was stirred at room temperature for 1.5 h and at 35 °C for 1 day. Then, the mixture was left at 80 °C for 2 days before product recovery and calcination at 540 °C. The molar ratio of the precursor mixture was 10 TEOS/10 $ZrOCl_2$/0.17 P123/57 HCl/1600 H_2O. This sample was termed ZrSBA-15.

Characterization. Powder X-ray diffraction (XRD) data were recorded on a Siemens D5000 θ-θ diffractometer (45 kV, 40 mA) using nickel-filtered Cu Kα radiation with wavelength $\lambda = 1.5406$ Å. Diffraction patterns were collected under ambient conditions in the 2θ range of 1.5° to 40.0° with a resolution of 0.04°. Analysis of ZrSBA-15 was carried out through small-angle X-ray scattering (SAXS) on a Siemens small-angle diffractometer with a Siemens HI-STAR area detector, operating at 40 kV and 30 mA ($\lambda = 1.5406$ Å).

Nitrogen adsorption isotherms were obtained at 77 K on a Micromeritics ASAP 2010 Gas Sorption and Porosimetry system. Samples were normally prepared for measurement by degassing at 150 °C under vacuum until a final pressure of 1×10^{-3} Torr was reached. BET surface areas were determined over a relative pressure range of 0.05 to 0.20.[24] Pore size distributions were calculated using the HK (Horváth-Kawazoe) method.[25]

Transmission electron micrographs (TEM) were taken on a JEOL 2000FX transmission electron microscope equipped with a lanthanum hexaboride (LaB_6) gun operating at an accelerating voltage of 200 kV and with an objective aperture of 50 μm. Samples for TEM studies were ground and sprinkled onto a carbon-coated copper grid.

(18) Jones, D. J.; Jiménez-Jiménez, J.; Jiménez-López, A.; Maireles-Torres, P.; Olivera-Pastor, P.; Rodriguez-Castellón, E.; Rozière, J. *Chem. Commun.* **1997**, 431.

(19) Tuel, A.; Gontier, S.; Teissier, R. *Chem. Commun.* **1996**, 651. (b) Gontier, S.; Tuel, A. *Appl. Catal. A* **1996**, *143*, 125.

(20) Occelli, M. L.; Biz, S.; Auroux, A. *Appl. Catal. A: Gen.* **1999**, *183*, 231.

(21) Huo, Q.; Margolese, D. I.; Ciesla, U.; Feng, P.; Gier, T. E.; Sieger, P.; Leon, R.; Petroff, P. M.; Schüth, F.; Stucky, G. D. *Nature* **1994**, *368*, 317. (b) Huo, Q.; Margolese, D. I.; Ciesla, U.; Demuth, D. G.; Feng, P.; Gier, T. E.; Sieger, P.; Firouzi, A.; Chmelka, B. F.; Schüth, F.; Stucky, G. D. *Chem. Mater.* **1994**, *6*, 1176.

(22) Zhang, W.; Wang, J.; Tanev, P. T.; Pinnavaia, T. J. *Chem. Commun.* **1996**, 979.

(23) Zhao, D.; Feng, J.; Huo, Q.; Melosh, N.; Fredrickson, G. H.; Chmelka, B. F.; Stucky, G. D. *Science* **1998**, *279*, 548. (b) Zhao, D.; Huo, Q.; Feng, J.; Chmelka, B. F.; Stucky, G. D. *J. Am. Chem. Soc.* **1998**, *120*, 6024.

(24) Gregg, S. K.; Sing, K. S. W. *Adsorption, Surface Area and Porosity*, 2nd ed.; Academic Press: London, 1982. (b) Webb, P. A.; Orr, C. *Analytical Methods in Fine Particle Technology*; Micromeritics Instrument Co.: Norcross, 1997.

(25) Horváth, G.; Kawazoe, K. *J. Chem. Eng. Jpn.* **1983**, *16*, 470.

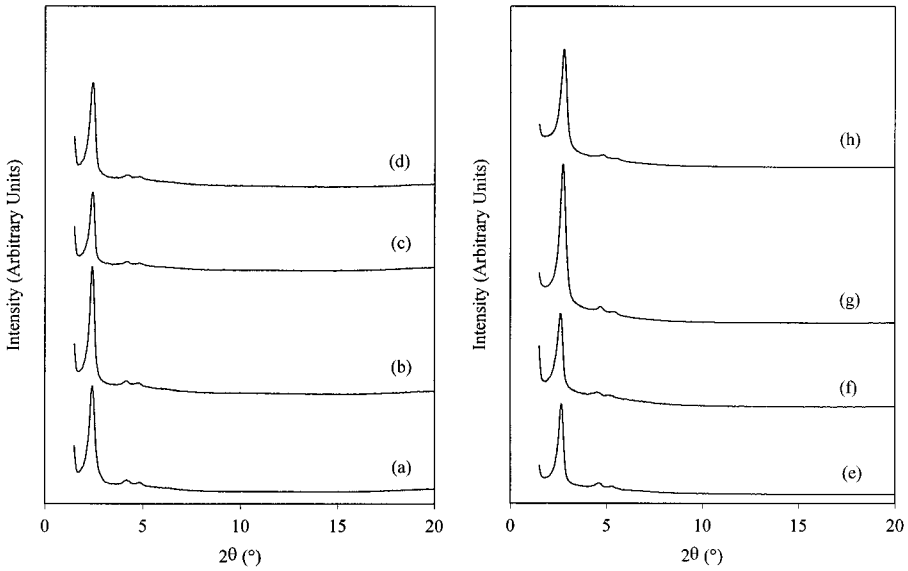

Figure 1. XRD patterns of as-synthesized (a) ZrSi1-0, (b) ZrSi1-1, (c) ZrSi1-3, and (d) ZrSi1-10; and of (e) ZrSi1-0, (f) ZrSi1-1, (g) ZrSi1-3, and (h) ZrSi1-10, after calcination at 540 °C.

Fourier transform infrared (FTIR) spectroscopy was performed on a Bio-Rad FTS-60A/896 spectrometer. An MTEC model 200 photoacoustic (PA) cell allowed nondestructive characterization of the powder samples.[26] PA-FTIR spectra were collected at a scan speed of 5 kHz for wavenumbers of 400 to 4000 cm^{-1} with a resolution of 4 cm^{-1}. Samples were purged under a stream of helium (99.999+%).

Diffuse reflectance UV−Vis spectra were collected on a Cary 5E UV−Vis−NIR spectrophotometer equipped with a Varian diffuse reflectance integrating sphere accessory. Halon was used as a background, and ZrO_2 (99+%, 100% monoclinic phase, Strem) was used as a reference sample. The Kubelka−Munk formalism $F(R_\infty) = (1 - R_\infty)^2/(2R_\infty)$ was used, where R_∞ is the reflectance at infinite thickness.[27] The optical absorption edge energy for allowed electron transitions, or band gap energy E_g, was determined by finding the x-intercept of the straight line in the low energy rise of a plot of $[F(R_\infty)h\nu]^2$ against $h\nu$, where $h\nu$ is the incident photon energy.

Thermogravimetric analysis (TGA) was performed on a Perkin-Elmer series 7 Thermal Analysis system. A ramp rate of 5 °C/min was used. Purified nitrogen (99.999+%) was employed as the purge gas.

Bulk elemental analysis through inductively coupled plasma atomic emission spectroscopy (ICP-AES) was performed by QTI (Whitehouse, NJ). Solid-state ^{29}Si cross-polarization magic angle spinning nuclear magnetic resonance (CP/MAS-NMR) spectra were collected at a frequency of 53 MHz and a CP contact time of 2 ms by Spectral Data Services, Inc. (Champaign, IL). Samples were spun at 4.0 kHz. Tetramethylsilane was used as the external reference. Surface composition analysis was carried out via X-ray photoelectron spectroscopy on a Surface Science ESCA spectrometer (model SSX-100) using Al Kα radiation.

Catalytic Testing. ZrSi was studied for the gas-phase acid-catalyzed isomerization of 1-butene. Twenty milligrams of ZrSi powder was placed in the middle of a single-pass, downflow quartz reactor. After the sample was activated under air at 500 °C for 1 h and cooled to 350 °C, the catalyst was contacted with a stream of 12% 1-butene in He at 350 °C and 1 atm. The 1-butene feed gas was 99.2+% pure (BOC), with mostly *n*-butane and isobutane as the impurities. The weight-hourly space velocity (WHSV) was 15 h^{-1}. The reaction pressure was 1 atm. Comparison of product distributions over ZrSi2-10 and commercial sulfated zirconia (calcined at 600 °C, MEI) was studied with 50 mg catalyst using a feed of 10.6% 1-butene in He (WHSV of 5.3 h^{-1}). The effluent was analyzed with a gas-sampling valve-enabled HP 6890 series plus GC (gas chromatograph) with a flame induction detector (FID) and a HP-PLOT/Al_2O_3/KCl-deactivated capillary column (ID = 0.32 mm; length = 50 m). The initial measurements were made 30 s after introduction of the 1-butene stream. Minor amounts of cracking products were detected, in addition to the isomerization products. Isobutene selectivity was based on total linear butenes available (1-butene + 2-butenes), as 2-butenes could also undergo skeletal isomerization to isobutene. The loss of detectable gas-phase products was attributed to their adsorption on the catalyst surface as carbonaceous deposits via coke formation.

The liquid-phase epoxidation of *cis*-cyclooctene was tested over ZrSi. A Teflon septum-sealed 25-mL flask was charged with 4 mL of dichloromethane (Mallinckrodt), 7.7 mmol of *cis*-cyclooctene (Lancaster), 0.5 mmol of *tert*-butyl hydroperoxide (TBHP, 5 M in decane, Aldrich), with 100 μL of chlorobenzene (Sigma-Aldrich) as the internal standard. An amount of catalyst was added such that the total Zr charged was 24 μmol. Fifty milligrams of pure mesoporous silica ZrSi1-0 was used as a reference. The flask was placed in a 40 °C silicone oil bath, and the reaction mixture was magnetically stirred. Samples were analyzed with a HP 5890 series II GC equipped with a FID and a HP-1 capillary column (ID = 0.25 mm; length = 30 m). Turnover frequency (TOF) was calculated based on the initial reaction rate of TBHP, the limiting reagent.

Results and Discussion

Effect of Zirconium Doping on ZrSi1 Mesostructure Synthesized under Low pH Condition. ZrSi1 materials were able to accommodate the larger Zr cation (r_{Zr} = 0.86 Å vs r_{Si} = 0.40 Å[28]) in the silica-based framework with little change to the long-range ordering before or after calcination (Figure 1). The hexagonal phase was ascertained from the *d*-spacings of the three observed XRD peaks, which corresponded to the relation $d_{hk0} = d_{100}/(h^2 + hk + k^2)^{1/2}$, where d_{100} is the *d*-spacing value of the main XRD peak. When doped with ≥ 2.8 wt % Zr, the silica-based framework of ZrSi1 contracted slightly more after calcination (Table 2). This can be

(26) McClelland, J. F.; Jones, R. W.; Luo, S.; Seaverson, L. M. In *Practical Sampling Techniques for Infrared Analysis*; Coleman, P. B., Ed.; CRC Press: Boca Raton, 1993; p 107.

(27) Delgass, W. N.; Haller, G. L.; Kellerman, R.; Lunsford, J. H. *Spectroscopy in Heterogeneous Catalysis*; Academic Press: New York, 1979.

(28) Shannon, R. D.; Prewitt, C. T. *Acta Crystallogr.* **1969**, *B25*, 925.

Table 2. Physical Properties of ZrSi Materials

sample	As-synthesized: d_{100} (Å)	calcined: d_{100} (Å)	framework contraction (Å)[a]	contraction (%)[b]	BET SA (m^2/g)	HK pore size (Å)	pore wall thickness (Å)[c]	pore volume (cm^3/g)
ZrSi1-0	36.5	33.2	3.8	9	1250	25	13	0.70
ZrSi1-0.2	35.7	32.7	3.5	8	1271	25	13	0.76
ZrSi1-1	36.4	33.2	3.7	9	1193	22	16	0.68
ZrSi1-3	36.4	32.2	4.8	12	1003	22	15	0.53
ZrSi1-10	36.1	31.6	5.2	12	1066	22	14	0.54
ZrSi2-0.1	42.1	38.0	4.7	10	1350	28	16	0.88
ZrSi2-0.2	41.2	36.5	5.4	11	1332	28	14	0.82
ZrSi2-0.4	39.4	36.5[d]	3.3	7	1269	23	19	0.68
ZrSi2-1	38.4	28.4	11.5	26	744	16	17	0.33
ZrSi2-3	38.4	26.4	13.9	31	473	16	14	0.24
ZrSi2-10	37.4	25.8	13.4	31	436	16	14	0.23
ZrSi1-3C	35.6	31.7	4.5	11	1150	21	16	0.63
ZrSBA-15	116[e]	111[e]	5.8	4	942	80	48	1.26

[a] Contraction = a_0(as-synthesized) − a_0(calcined), where a_0 is the center-to-center repeat distance ($2d_{100}/\sqrt{3}$). [b] Percent change in a_0 after calcination at 540 °C. [c] Wall thickness = a_0(calcined) − (HK pore size). [d] Shoulder on main peak found (d-spacing = 30.0 Å). [e] Determined through SAXS instead of XRD.

attributed to the octahedrally coordinated Zr cation's capacity to form more metal−oxygen bonds than tetrahedrally coordinated Si, increasing the degree of condensation. TEM studies confirmed the long-range, hexagonal pore packing of ZrSi1 (Figure 2a−c). Pore sizes as determined from TEM images are about 25 ± 5 Å. The uncertainty arises from the high dependency of observed pore size on sample thickness and imaging focus.[29] The doped ZrSi1-x materials, where x = 1, 3, and 10, had pores of 22 Å by HK analysis, which were slightly smaller than the pores in undoped silica (25 Å) (Table 2).

Materials with a Zr content < 2.8 wt % were somewhat similar structurally to undoped ZrSi1-0. ZrSi1-0.2 had a slightly smaller mesostructure as compared to ZrSi1-0, based on the smaller value of d_{100}-spacing, but its framework contracted to a similar extent as ZrSi1-0 after calcination. Calcined ZrSi1-0 and ZrSi1-0.2 essentially had the same structural characteristics (Table 2). ZrSi1-1 contained more Zr and had a smaller pore size and thicker pore walls, but it also contracted as much as ZrSi1-0 or ZrSi1-0.2.

The ZrSi1 materials exhibited type IV nitrogen adsorption−desorption isotherms, representative of mesoporous materials (Figure 3a−d). These materials did not display hysteresis in their nitrogen adsorption−desorption isotherms. Hysteresis is usually observed in mesoporous materials due to capillary condensation in the open-ended pore channels.[24] While there is no clear explanation still, a critical diameter (~40 Å) exists below which hysteresis in the nitrogen isotherm disappears.[30,31]

Effect of Zirconium Doping on ZrSi2-x ($x \geq 1$) Mesostructure Synthesized under Higher pH Condition. ZrSi2 materials prepared at pH = 0.75 had a higher Zr content (≥ 10.7 wt %) and were structurally different from ZrSi1 materials prepared at pH = −0.25. The as-synthesized ZrSi2 materials prepared at pH = 0.75 were also of a hexagonal phase (Figure 4a−c), but their d_{100}-spacings were slightly larger than those of as-synthesized ZrSi1 materials (Table 2). Since the as-synthesized materials in the ZrSi2 series had fairly similar d_{100}-spacings despite the large differences in Zr content (Table 1), the relatively larger d_{100}-spacings of as-synthesized ZrSi2 materials (as compared to ZrSi1 materials) were attributed to the difference in synthesis pH.

After calcination, the ZrSi2 materials contracted more than twice that of ZrSi1 (26−31% vs 8−12%), resulting in smaller pore sizes (Figure 4d−f and Table 2). The calcined ZrSi2 materials were microporous rather than mesoporous, as represented by the type I nitrogen adsorption−desorption isotherms (Figure 3e−g). Formation of microporous materials through such a large contraction is uncommon; a microporous phosphated zirconia material prepared in such a manner was previously reported.[32] Typically, the supramolecular templating of microporous materials requires very short amphiphilic molecules.[33,34] TEM studies showed that the ZrSi2 structure was made up of small regions of hexagonally ordered micropores (Figure 2d−f). There was probably some loss of porous structure as shown by the less intense XRD peaks of the calcined materials, in addition to loss in long-range ordering after calcination as shown by the disappearance of the higher-order XRD peaks (Figure 4d−f). The small rise detected in the nitrogen isotherms near a relative pressure of 0.99 was indicative of interparticle porosity.[24]

Effect of Zirconium Doping on ZrSi2-x ($x < 1$) Mesostructure Synthesized under Higher pH Condition. Synthesis at pH = 0.75 favored greater Zr incorporation than synthesis at pH = −0.25 and resulted in materials (ZrSi2-x, $x \geq 1$) that exhibited severe framework contraction after calcination. Thus, the preparation of ZrSi2-x materials, where x = 0.1, 0.2 and 0.4, was investigated. These ZrSi2-x materials were found to contain ~1−6 wt % Zr; they exhibited strong low-angle XRD peaks as compared to pure silica ZrSi2−0, which showed no XRD peak (Figure 5a−d). Three XRD sharp peaks indicative of a hexagonal phase were found for ZrSi2-0.4, but only a broad peak was noted for ZrSi2-0.1 and ZrSi2-0.2. The d_{100} value was observed

(29) Chen, C.-Y.; Xiao, S.-Q.; Davis, M. E. *Microporous Mater.* **1995**, *4*, 1. (b) Schacht, S.; Janicke, M.; Schüth, F. *Microporous Mesoporous Mater.* **1998**, *22*, 485.
(30) Sonwane, C. G.; Bhatia, S. K.; Calos, N. *Ind. Eng. Chem. Res.* **1998**, *37*, 2271.
(31) Inoue, S.; Hanzawa, Y.; Kaneko, K. *Langmuir* **1998**, *14*, 3079.
(32) Ciesla, U.; Schacht, S.; Stucky, G. D.; Unger, K. K.; Schüth, F. *Angew. Chem., Int. Ed. Engl.* **1996**, *35*, 541. (b) Ciesla, U.; Fröba, M.; Stucky, G.; Schüth, F. *Chem. Mater.* **1999**, *11*, 227.
(33) Wong, M. S.; Ying, J. Y. *Chem. Mater.* **1998**, *10*, 2067.
(34) Sun, T.; Ying, J. Y. *Nature* **1997**, *389*, 704. (b) Sun, T.; Wong, M. S.; Ying, J. Y. *Chem. Commun.* **2000**, 2057.

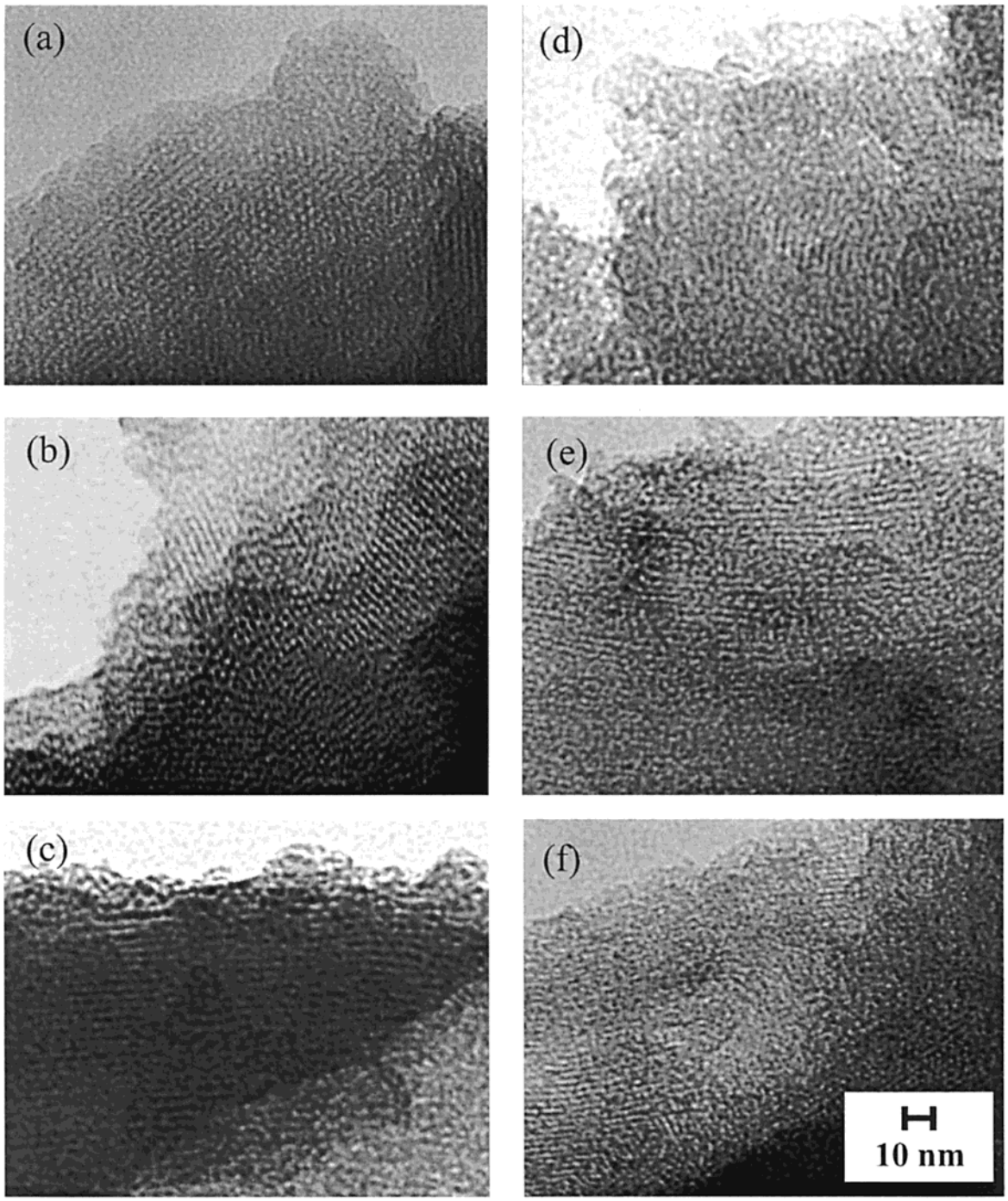

Figure 2. TEM images of (a) ZrSi1-1, (b) ZrSi1-3, (c) ZrSi1-10, (d) ZrSi2-1, (e) ZrSi2-3, and (f) ZrSi2-10, after calcination at 540 °C.

to be highest in as-synthesized ZrSi2-*x* with a low Zr content.

Broad, low-angle XRD peaks were found for ZrSi2-0.1, ZrSi2-0.2, and ZrSi2-0.4 after calcination at 540 °C, indicating the retention of a mesostructure (Figure 5e−g). These ZrSi2 materials (∼1−6 wt % Zr) contracted about 7−10%, less than the 26−31% found for ZrSi2-*x* containing > 10 wt % Zr (Table 2). The decreased amount of contraction in the low-Zr containing ZrSi2-*x* materials ($x = 0.1-0.2$), coupled with their larger mesostructures, resulted in pore sizes larger than that in the pure mesoporous silica ZrSi1-0 (Table 2); the surface areas and pore volumes were found to be larger as well. ZrSi2-0.4 calcined at 540 °C showed a small shoulder near the main XRD peak, indicating that either a nonhexagonal phase or a mixture of phases was formed upon calcination (Figure 5g).

Control of Zirconium Doping in ZrSi Materials. The incorporation of zirconium in the framework of mesoporous silica depended on the amounts of Zr precursor and HCl added to the synthesis mixture, as summarized in Table 1. Under highly acidic conditions (pH = −0.25), small amounts of Zr were incorporated into mesoporous silica (1.0−4.4 wt % Zr). The loadings were similar to those achieved through the other synthesis routes.[18,19] The Zr content in these ZrSi1 powders was far lower than that expected for 100% product recovery, indicating that much of the $Zr(SO_4)_2$

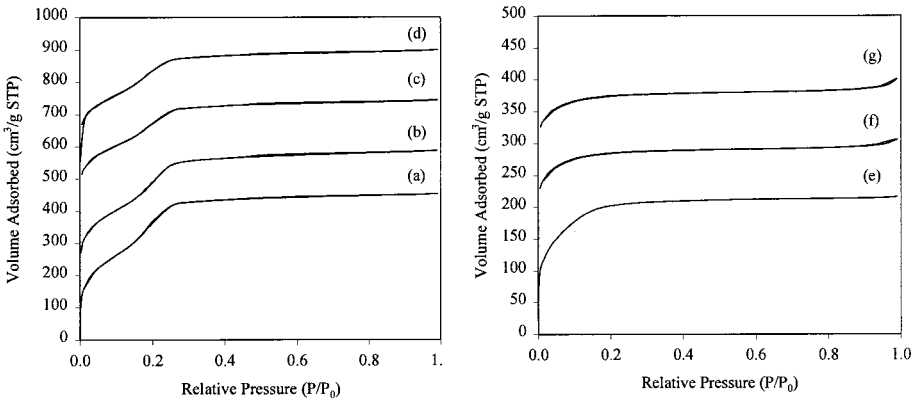

Figure 3. Nitrogen adsorption−desorption isotherms of (a) ZrSi1-0, (b) ZrSi1-1, (c) ZrSi1-3, (d) ZrSi1-10, (e) ZrSi2-1, (f) ZrSi2-3, and (g) ZrSi2-10, after calcination at 540 °C. Isotherms were offset for clarity.

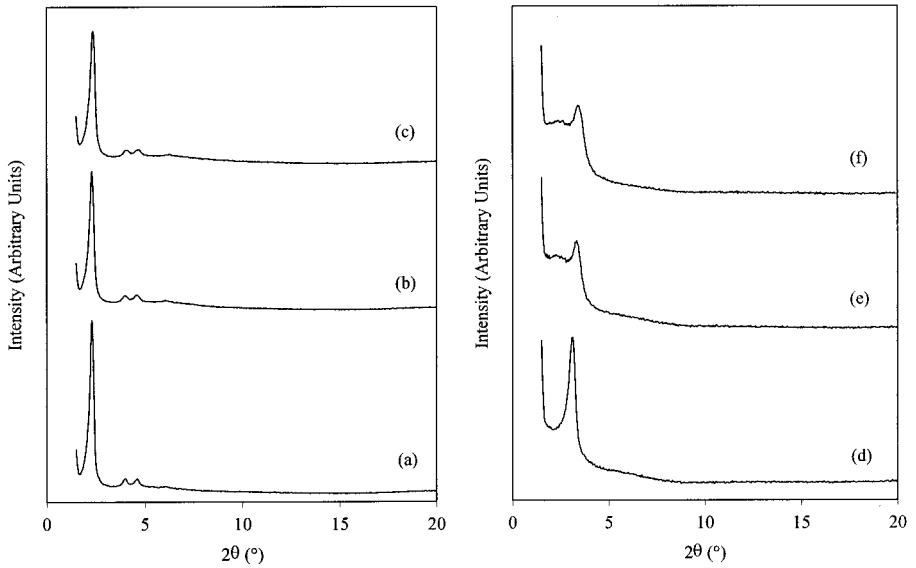

Figure 4. XRD patterns of as-synthesized (a) ZrSi2-1, (b) ZrSi2-3, and (c) ZrSi2-10; and of (d) ZrSi2-1, (e) ZrSi2-3, and (f) ZrSi2-10, after calcination at 540 °C.

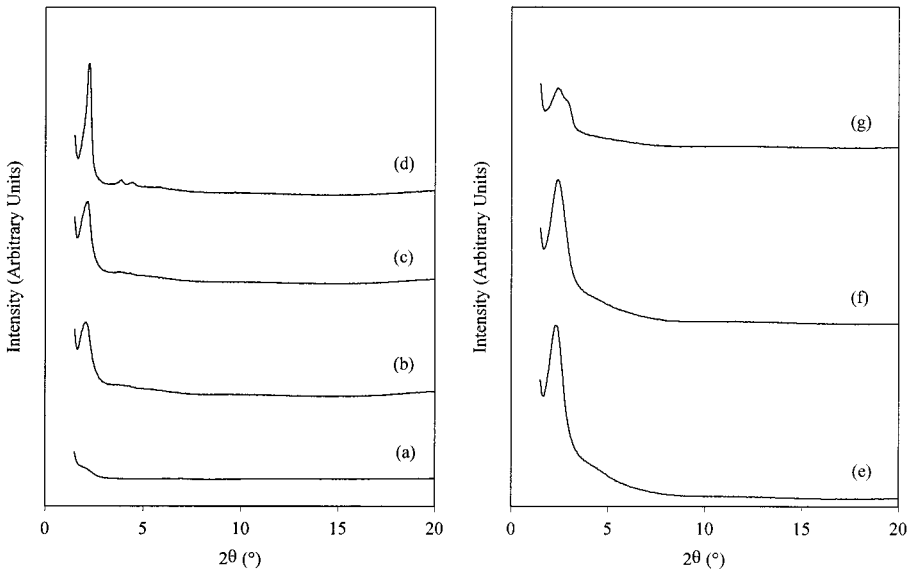

Figure 5. XRD patterns of as-synthesized (a) ZrSi2-0, (b) ZrSi2-0.1, (c) ZrSi2-0.2, and (d) ZrSi2-0.4; and of (e) ZrSi2-0.1, (f) ZrSi2-0.2, and (g) ZrSi2-0.4, after calcination at 540 °C.

precursor in the synthesis mixtures was not incorporated into the silica-surfactant mesostructure.

The Zr content in the ZrSi2 materials prepared at pH = 0.75 was much higher and closer to the expected doping values (Table 1). Reducing the HCl amount by 10 times led to an approximately 5-fold increase in Zr content, whereas increasing the Zr precursor amount by 10 times only roughly doubled the Zr content; this

Table 3. Sulfur Content of Selected ZrSi Materials

sample	measured Zr content (wt %)	measured S content (wt %)	S/Zr molar ratio	calc sulfate surface density (SO_4^{2-}/nm^2)
ZrSi1-0	0.0	0.00	0.00	0.00
ZrSi1-1	2.0	<0.10[a]	<0.01	<0.01
ZrSi1-10	4.4	0.14	0.09	0.03
ZrSi2-1	10.7	0.52	0.14	0.13
ZrSi2-10	19.6	1.33	0.19	0.57
SZ[b]	74.0[c]	1.61	0.06	3.22

[a] Below detection limit. [b] Sulfated zirconia (calcined at 600 °C; SA = 94 m^2/g; MEI). [c] Calculated Zr amount in ZrO_2.

observation did not hold for ZrSi1-*x* and ZrSi2-*x* materials, where $x < 1$. Combining these two effects increased the Zr content by ∼10 times, from 2.0 to 19.6 wt % Zr. Such a high dopant loading in nanoporous silica has not been reported previously.

Clearly, a higher pH has a greater impact on Zr incorporation than a higher Zr precursor amount. The nature of Zr salts is known to be sensitive to solution pH.[35] The $Zr(SO_4)_2$ precursor exists as a polymeric species in solution and, under extremely low pH's, it can exist as monomeric species.[36] Thus, the $Zr(SO_4)_2$ species that entered the templated mesostructure at the two different synthesis pH's might be significantly different. It was noted that, during the synthesis, there was no measurable change in the pH of the HCl/CTAB solution upon addition of the Zr salt.

The ZrSi2-0.4 sample had a measured Zr content that was slightly higher than the theoretical amount (Table 1). The formation of a second phase in ZrSi2-0.4 that is enriched in Zr may be postulated (Figure 5g), resulting in the relative increase in Zr amount.

Calcined ZrSi materials consisting of > 4 wt % Zr were found to contain trace amounts of sulfur, presumably in the form of surface sulfates remaining from the $Zr(SO_4)_2$ precursor (Table 3). FTIR bands for sulfate groups (900−1400 cm^{-1}) were not detected, though, because of overlap with infrared bands of SiO_2 (Figure 6).[15a] The sulfate surface coverage of ZrSi materials was very low (≤0.57 SO_4^{2-}/nm^2) as compared to sulfated zirconia (SZ) (3.22 SO_4^{2-}/nm^2), a solid acid material known for its very strong acidity.[37] Surface sulfates have been found to generate strong acid sites on zirconia−silica composites also.[15]

ZrSi could be prepared without the sulfates by using $ZrOCl_2$ instead of $Zr(SO_4)_2$. Interestingly, at the same precursor Zr/Si ratio of 0.3, a higher Zr loading resulted with $ZrOCl_2$ than with $Zr(SO_4)_2$ (cf. 4.5 wt % in ZrSi1-3C and 2.8 wt % in ZrSi1-3). A higher precursor Zr/Si ratio of 1.0 using $Zr(SO_4)_2$ was required for a comparable amount of Zr incorporation (4.4 wt % in ZrSi1-10).

Nature of Zirconium in the Framework. Several techniques were used to provide insight into the nature of Zr in the silica-based framework. The PA-FTIR spectrum of ZrSi1-0 (Figure 6a) showed the phonon band structure of pure SiO_2: 460 cm^{-1} (O−Si−O bending), 620 cm^{-1} (Si−O−Si deformation), 815 cm^{-1} (symmetric Si−O−Si stretching), 980 cm^{-1} (Si−OH stretching), 1000−1240 cm^{-1} (antisymmetric Si−O−Si stretching), 1625 cm^{-1} (molecular H_2O bending), and 1860 cm^{-1} (SiO_2 overtone).[38] Subtle changes in the PA-FTIR spectra were observed with increasing Zr dopant amount (Figure 6). The Si−OH stretching peak at 980 cm^{-1} broadened, suggesting interaction between the surface silanol groups with neighboring Zr cations. This effect of Zr has been previously observed in metal-doped zeolites.[16] A shoulder peak developed between 880 and 980 cm^{-1}, which was attributed to the Si−O stretching in Si−O−Zr heterolinkages.[39] No separate zirconia phase was found in the ZrSi materials, which would exhibit a broad infrared band at ∼520 cm^{-1} for the tetragonal ZrO_2 phase.[40]

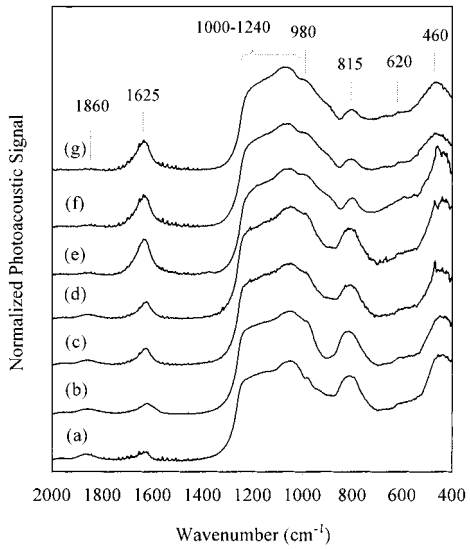

Figure 6. PA-FTIR spectra (low-wavenumber region) of (a) ZrSi1-0, (b) ZrSi1-1, (c) ZrSi1-3, (d) ZrSi1-10, (e) ZrSi2-1, (f) ZrSi2-3, and (g) ZrSi2-10, after calcination at 540 °C.

The hydroxyl groups were detected in the ZrSi materials (Figure 7). A peak at 3745 cm^{-1} was observed in the spectrum of undoped mesoporous silica, indicating the presence of isolated silanol (Si−OH) groups. These groups were associated with Q^2 and Q^3 Si cations as geminal and single silanols, respectively.[41] The notation Q^n denotes the bonding environment of the central Si in $(SiO)_n$−Si−$(OH)_{4-n}$, where n = 0−4. The broad absorption band in Figure 7 corresponded to silanols hydrogen-bonded with neighboring silanol groups (∼3530 cm^{-1}) and with adsorbed water (3000−3700 cm^{-1}). Such hydrogen bonding interactions involving different populations of silanols were reported to exist in pure silicate MCM-41.[42] The position and intensity of the isolated and hydrogen-bonded silanol peaks remained essentially unchanged in the ZrSi1 materials, indicating little effect of Zr doping. ZrSi2 materials showed a much less intense 3745 cm^{-1} peak, indicating a smaller population of isolated silanol groups. Conversely, the broad 3000−3700 cm^{-1} band of ZrSi2 was more intense from the

(35) Cotton, F. A.; Wilkinson, G. *Advanced Inorganic Chemistry: A Comprehensive Text*, 5th ed.; John Wiley: New York, 1988.
(36) Clearfield, A.; Serrette, G. P. D.; Khazi-Syed, A. H. *Catal. Today* **1994**, *20*, 295.
(37) Song, X.; Sayari, A. *Catal. Rev.-Sci. Eng.* **1996**, *38*, 329. (b) Cheung, T.-K.; Gates, B. C. *Chemtech* **1997**, *9*, 28.
(38) Ying, J. Y.; Benziger, J. B.; Navrotsky, A. *J. Am. Ceram. Soc.* **1993**, *76*, 2571.
(39) Lee, S. W.; Condrate, R. A., Sr. *J. Mater. Sci.* **1988**, *23*, 2951.
(40) Debsikdar, J. C. *J. Non-Cryst. Solids* **1986**, *87*, 343.
(41) Burneau, A.; Gallas, J.-P. In *The Surface Properties of Silicas*; Legrand, A. P., Ed.; John Wiley and Sons: Chichester, 1998; p 147.
(42) Chen, J.; Li, Q.; Xu, R.; Xiao, F. *Angew. Chem., Int. Ed. Engl.* **1995**, *34*, 2694.

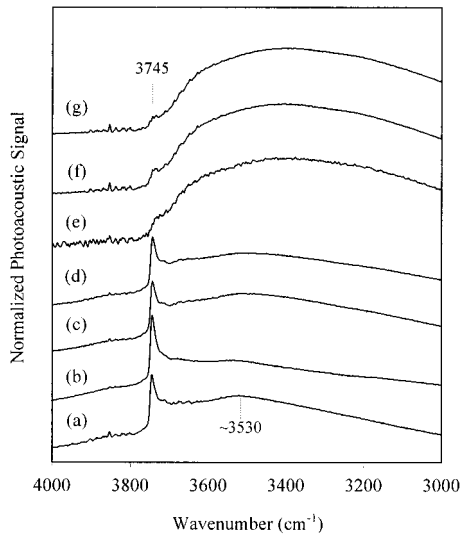

Figure 7. PA-FTIR spectra (high-wavenumber region) of (a) ZrSi1-0, (b) ZrSi1-1, (c) ZrSi1-3, (d) ZrSi1-10, (e) ZrSi2-1, (f) ZrSi2-3, and (g) ZrSi2-10, after calcination at 540 °C.

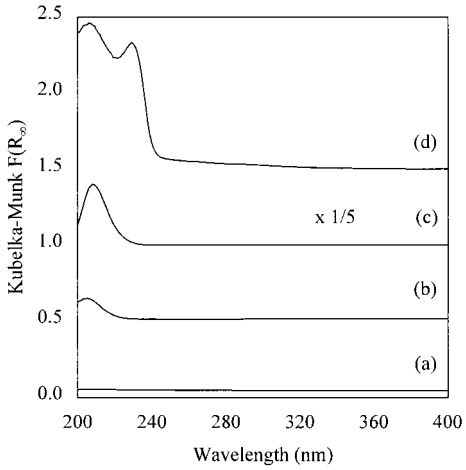

Figure 8. UV−Vis spectra of (a) ZrSi1-0, (b) ZrSi1-10, and (c) ZrSi2-10, after calcination at 540 °C, and (d) ZrO_2. Spectra were offset for clarity.

greater amounts of hydrogen-bonded silanol and adsorbed water, which were further evidenced by the 1625 cm^{-1} molecular water bending mode in Figure 6.

UV−Vis spectroscopy[19,43] provided insights into the local environment of zirconium cations within the silica-based matrix of representative ZrSi samples. The UV−Vis spectra of ZrSi1-10 and ZrSi2-10 (Figure 8b−c) did not resemble that of pure zirconia (Figure 8d), further corroborating the absence of a separate zirconia phase in the ZrSi materials. ZrSi1-0 was UV−Vis transparent (Figure 8a), as expected for pure silica. The single band in the absorption spectra of ZrSi1-10 and ZrSi2-10 represented an O → Zr ligand-to-metal charge transfer (LMCT) transition.[44] This band blue-shifted to lower wavelengths as compared to pure zirconia, which corresponded to larger band gap energies for Zr-doped silicas than for zirconia (Table 4).[27] The blue-shifting also indicated the lack of bulk zirconia in ZrSi materials

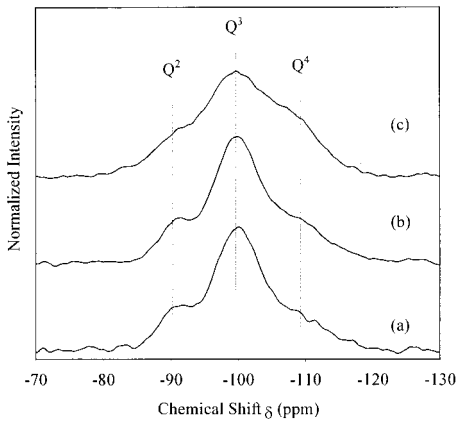

Figure 9. ^{29}Si CP/MAS-NMR spectra of (a) ZrSi1-0, (b) ZrSi1-10, and (c) ZrSi2-10, after calcination at 540 °C.

Table 4. UV-Vis Maxima and Bandgap Energies of Representative ZrSi Materials

sample	Zr content (wt %)	band max (nm)	E_g (eV) (±0.05)
ZrSi1-0	0.0	N/A	N/A
ZrSi1-10	4.4	205	5.75
ZrSi2-10	19.6	208	5.65
ZrO_2	74.0	206, 229	5.20

and implicated the presence of either isolated zirconium cations or highly dispersed zirconium oxide species.[16,45] Zirconium oxide species in sol−gel derived zirconia−silica composites were reported to be in the form of ultrafine, amorphous clusters.[45a] ZrSi2-10 had a smaller band gap energy than ZrSi1-10, indicating larger zirconium oxide species were formed at higher Zr loadings.

^{29}Si CP/MAS-NMR was performed on representative samples of ZrSi to examine qualitatively how Zr perturbed the local bonding environment of surface Si. The ^{1}H-^{29}Si CP technique intensifies the NMR signal of Si atoms near protons, and so it is useful in studying the Si atoms located at or near the pore wall surface.[46,47] ZrSi1-0, ZrSi1-10, and ZrSi2-10 were found to contain three types of Si: Q^2 (−90 ppm), Q^3 (−99 ppm), and Q^4 (−109 ppm) (Figure 9). It is assumed that the Q^2 and Q^3 Si atoms are exposed directly at the surface, as silanol groups are unlikely to reside within the thin pore walls (as internal Q^3 Si) without diminishing structural integrity. The Q^4 Si atoms can lie within the framework or at the surface.[48] The amount of Si bonded to Zr, e.g., $(SiO)_2-Si-(OZr)_2$ and $(SiO)_3-Si-OZr$, could not be determined through ^{29}Si CP/MAS-NMR and would be difficult to measure quantitatively with ^{29}Si MAS-NMR because of overlapping resonance peaks with Q^2 and Q^3 Si sites, respectively.[49,50]

The similarity between the Si site ratios of ZrSi1-0 and ZrSi1-10 showed that the incorporation of 4.4 wt % Zr did not significantly alter the population of surface

(43) Morey, M. S.; Stucky, G. D.; Schwarz, S.; Fröba, M. *J. Phys. Chem. B* **1999**, *103*, 2037.
(44) Schoonheydt, R. A. In *Characterization of Heterogeneous Catalysts*; Delannay, F., Ed.; Marcel Dekker: New York, 1984; p 125.
(45) Moon, S.-C.; Fujino, M.; Yamashita, H.; Anpo, M. *J. Phys. Chem. B* **1997**, *101*, 369. (b) Gao, X.; Fierro, J. L. G.; Wachs, I. E. *Langmuir* **1999**, *15*, 3169.
(46) Engelhardt, G.; Koller, H. In *Solid-State NMR II − Inorganic Matter*; Blumich, B., Ed.; Springer-Verlag: Berlin, 1994; p 1.
(47) Zhao, X. S.; Lu, G. Q.; Whittaker, A. K.; Millar, G. J.; Zhu, H. Y. *J. Phys. Chem. B* **1997**, *101*, 6525.
(48) Steel, A.; Carr, S. W.; Anderson, M. W. *Chem. Mater.* **1995**, *7*, 1829.
(49) Terry, K. W.; Lugmair, C. G.; Tilley, T. D. *J. Am. Chem. Soc.* **1997**, *119*, 9745.
(50) Andrianainarivelo, M.; Corriu, R.; Leclercq, D.; Mutin, P. H.; Vioux, A. *J. Mater. Chem.* **1996**, *6*, 1665.

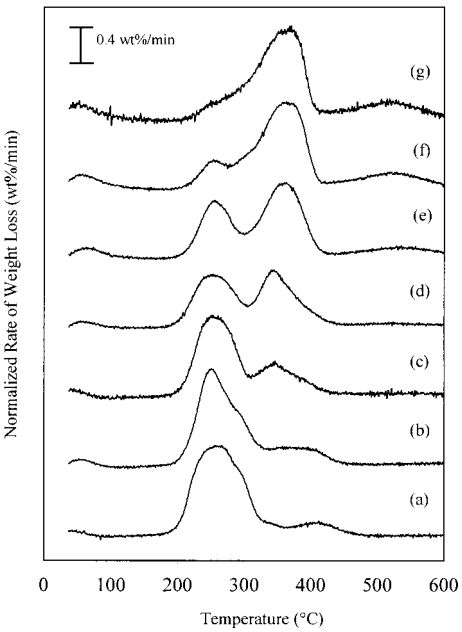

Figure 10. Derivative of TGA weight loss profiles (under flowing nitrogen) of as-synthesized (a) ZrSi1-0, (b) ZrSi1-1, (c) ZrSi1-3, (d) ZrSi1-10, (e) ZrSi2-1, (f) ZrSi2-3, and (g) ZrSi2-10. Profiles were offset for clarity.

Table 5. Relative ^{29}Si CP/MAS-NMR Peak Areas and Chemical Shifts of Representative ZrSi Materials

sample	Zr content (wt %)	% Q^2 Si sites	% Q^3 Si sites	% Q^4 Si sites
ZrSi1-0	0.0	16.5	58.2	25.3
ZrSi1-10	4.4	15.1	60.8	24.1
ZrSi2-10	19.6	16.3	44.0	39.7

Si species of the pure silica framework (Table 5). On the other hand, ZrSi2-10 differed greatly from ZrSi1-0 and ZrSi1-10. The loss in Q^3 Si sites in ZrSi2-10 was consistent with the decrease in the PA-FTIR isolated silanol peak at 3745 cm^{-1} (Figure 7). A greater percentage of Q^4 Si atoms was detected in ZrSi2-10. PA-FTIR data (Figure 7) indicated an increase in the hydrogen bonding band, which could be attributed to hydroxyl groups associated with surface Zr cations; this suggested that the Q^4 atoms in ZrSi2-10 laid at the surface sites. Thus, the differences in the chemical environment of surface Si in ZrSi2-10 as compared to ZrSi1-0 or ZrSi1-10 might be ascribed to the more contracted, condensed framework of ZrSi2-10.

Surfactant−Framework Interactions in ZrSi. The strength of interactions between the surfactant and the framework, as a function of Zr doping, was studied through TGA under inert atmosphere. The weight loss of the undoped silica ZrSi1-0 was found to occur in two stages (Figure 10a). The broad peak at 260 °C denoted the loss of CTAB through pyrolysis, and the peak at 410 °C was attributed to the removal of carbonaceous deposits. With increasing Zr dopant amounts, the peak at 260 °C decreased and a new peak at ∼350 °C emerged and shifted to higher temperatures (Figure 10b−g). Thus, two populations of surfactant molecules with different bonding strengths were observed as a function of Zr loading. The more strongly bound CTAB surfactants, represented by the peak at the higher temperature of ∼350 °C, could be associated with Zr cations; and the less strongly bound surfactants, represented by the peak at 260 °C, could be associated with Si cations. This implied that the Zr precursor interacted with the surfactant during mesostructure formation. Analogous surfactant−framework interactions were found in mesoporous aluminum-doped silicas, whereby amine surfactants were bonded strongly to Al cations.[51]

Table 6. Bulk and Surface Zr Concentrations of Representative ZrSi Materials

sample	bulk Zr content (wt %)	surface Zr content (wt %)
ZrSi1-10	4.4	12.6
ZrSi2-10	19.6	25.5
ZrSi1-3C	4.5	9.4
ZrSBA-15	4.8	10.7

A third peak emerged at 520 °C in ZrSi2 materials with Zr amounts of ≥ 10.7 wt %, representing the loss of water of condensation from the severe contraction of the framework (Figure 10e−g). Total weight loss by 600 °C was ca. 56% for these ZrSi2 materials, as compared to ca. 47% for ZrSi1-0 pure silica and ZrSi1 materials.

Synthesis Mechanism. In the formation of pure mesoporous silica under low-pH conditions ($S^+X^-I^+$ pathway), it has been postulated that the anion X^- from the acid (or from the surfactant) mediated the electrostatic interplay between the positively charged headgroup of CTAB (S^+) and the positively charged Si precursor (I^+) hydrolyzed from TEOS.[21] Resultant mesoporous silica was reported to contain 2 wt % Cl, hinting at the active role Cl^- anions played in the synthesis.[52] In this manner, the low-pH synthesis route contrasted high-pH (S^+I^- pathway)[4] and neutral-pH (S^0I^0 pathway)[53] routes to mesoporous silicas. Through our Zr doping studies, we found that the synthesis of ZrSi materials supported the $S^+X^-I^+$ electrostatic interactions model, in which $S^+ = CTA^+$, $X^- = Cl^-/Br^-/SO_4^{2-}$, and $I^+ = Si^{4+}/Zr^{4+}$, but involved additional factors.

The quantity of Zr incorporated depended greatly on synthesis pH (Table 1), suggesting a pronounced sensitivity of Zr doping to the solution chemistry of Zr cations. It is known that Zr cations can exist in various solubilized forms, depending on their counteranions and pH.[35,36] As mentioned earlier, $Zr(SO_4)_2$ exists as a polymerized species in solution, with the SO_4^{2-} acting to complex multiple Zr cations.[36] At the lower synthesis pH of −0.25, the HCl/CTAB solution remained clear upon introduction of the $Zr(SO_4)_2$ solution. No precipitation was observed until TEOS addition. At the higher pH of 0.75, the solution became cloudy 2 h after combining with $Zr(SO_4)_2$. These observations indicated a stronger interaction between the $Zr(SO_4)_2$ and CTAB precursors at pH = 0.75 than at pH = −0.25, further supporting the connection between higher synthesis pH and higher Zr content.

Implied by direct interaction of $Zr(SO_4)_2$ and CTAB and by the presence of strongly bound CTAB, the preferential location of the Zr cation at the surface was substantiated by XPS results. The surface Zr content of representative ZrSi materials was found greater than the respective bulk Zr composition (Table 6).

(51) Mokaya, R.; Jones, W. *Chem. Commun.* **1996**, 981.
(52) Schacht, S.; Huo, Q.; Voigt-Martin, I. G.; Stucky, G. D.; Schüth, F. *Science* **1996**, *273*, 768.
(53) Tanev, P. T.; Pinnavaia, T. J. *Science* **1995**, *267*, 865.

In the synthesis of ZrSi2 materials, TEOS was immediately added after $Zr(SO_4)_2$ introduction to the HCl/CTAB solution. When TEOS was added 2 h after the introduction of $Zr(SO_4)_2$, a thermally unstable, hexagonally ordered precipitate resulted. When TEOS was withheld from the synthesis mixture, a thermally unstable, hexagonally ordered precipitate also resulted. This mesostructured zirconium oxide was similar to those studied by Ciesla et al., who reported their materials also lacked thermal stability.[32] These experiments indicated that SiO_2 provided the thermal stability lacking in a pure ZrO_2 framework, and that the TEOS precursor must be added before precipitation of the $Zr(SO_4)_2$/CTAB mesostructure (of which the formation was inhibited at pH = −0.25).

$ZrOCl_2$ precursor was found a more effective dopant than $Zr(SO_4)_2$ in the preparation of ZrSi1 materials at pH = −0.25 (Table 1). This might be due to tetrameric molecular species $[Zr_4(OH)_8(H_2O)_{16}]^{8+}$ in solution arising from dissolved $ZrOCl_2$.[35,36] In an analogous fashion as $Zr(SO_4)_2$ polymeric species, this tetrameric species was able to interact with CTAB, as suggested by the excess Zr on the surface of ZrSi materials (Table 6). However, the higher synthesis pH of 0.75 did not lead to precipitation when $ZrOCl_2$ was added to a HCl/CTAB solution, unlike the case of $Zr(SO_4)_2$. In fact, no precipitate was formed even after the addition of TEOS (yielding a clear solution of HCl/CTAB/$ZrOCl_2$/TEOS, pH = 0.75). Clearly, the sulfate played a crucial role in the Zr doping of mesostructured silica at the higher pH of 0.75.

Synthesis mixtures at pH = −0.25 and 0.75 differed not only in the amount of available protons, but also in the amount of Cl^- anions. The ion concentration, which can be characterized by ionic strength I ($= {}^1/_2\sum cz^2$, where c is concentration and z is valence charge), is different at the two different synthesis pH's (1.77 M at pH = −0.25 vs 0.18 M at pH = 0.75), and would impact the electrostatic interactions necessary for ZrSi formation. The effect of ion concentration was tested by adding an amount of KCl to a solution of HCl/CTAB/$ZrOCl_2$/TEOS (pH = 0.75), such that the total number of Cl^- anions was the same as that found in the synthesis mixture at pH = −0.25. A nonmesostructured precipitate resulted after 2 days of aging, indicating a high ion concentration could induce precipitation, but a sufficient amount of protons was necessary for supramolecular templating to take place under the higher pH of 0.75.

Gas-Phase 1-Butene Isomerization. 1-Butene isomerization is a useful reaction for probing the strength of acid sites.[54] Whereas the double-bond isomerization of 1-butene to *cis*-2-butene and *trans*-2-butene occurs over acid sites of moderate strength, skeletal isomerization to isobutene is catalyzed over strong acid sites in a separate reaction pathway (Figure 11a).

1-Butene isomerization was used to examine the effect of Zr loading on the acidity of ZrSi materials. Initial activities of the ZrSi materials were studied because of fairly rapid deactivation. The total conversion and skeletal isomerization of 1-butene increased with Zr doping level (Figure 12). This activity profile with increasing Zr doping amounts is commonly observed in mixed metal oxides and is attributed to increased

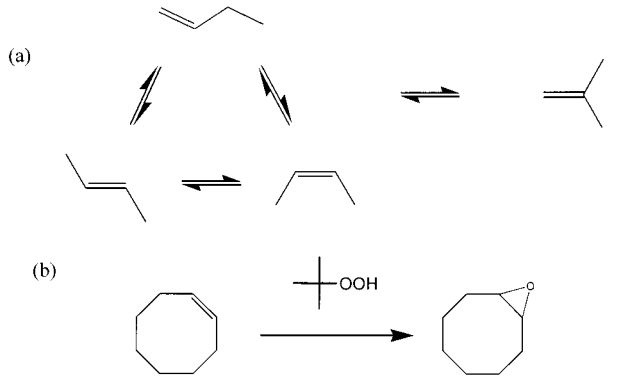

Figure 11. Reaction schemes of (a) 1-butene isomerization and (b) *cis*-cyclooctene epoxidation.

heterolinkages between Zr and Si cations.[13−15,55] An optimum number of Zr−O−Si and M′−O−M linkages generally leads to volcano-like behavior in catalytic activity and acidity found with zirconia-silica and other binary mixed metal oxides, respectively.[13] However, no such maximum in skeletal isomerization activity was observed with the ZrSi materials over the range of compositions examined.

In addition, there was some enhancing effect of SO_4^{2-} on the observed isomerization activity, as noted by other researchers with sulfated zirconia−silica materials.[15] As shown in Figure 12, the initial isomerization activity of the ZrSi1-3C sample (containing 4.5 wt % Zr with no sulfates) was found to be 50% that of ZrSi1-10, which contained 4.4 wt % Zr and 0.14 wt % S (Table 3). ZrSi1-3C had an ∼8% greater surface area than ZrSi1-10 (Table 2). The presence of sulfates at a low surface density of 0.03 SO_4^{2-}/nm^2 (Table 3) was sufficient to increase the catalytic activity of ZrSi1-10. While sulfates are known to create active sites on the surface of sulfated zirconia, the actual nature of the acid sites remains elusive, especially with sulfated zirconia−silica systems.[15,37] It is generally accepted, though, that the sulfates generate acid sites of the Brønsted type, which are active for acid catalysis. Brønsted acid sites are hydroxyl groups, but only a fraction of the hydroxyl groups present would contribute to Brønsted acidity.[56] For comparison, 0.03−0.57 SO_4^{2-}/nm^2 is much less than the surface density of hydroxyl groups for pure MCM-41 silicate (2.5−3.0 $SiOH/nm^2$,[47] as compared to 4.6 $SiOH/nm^2$ of amorphous silica[57]).

Conversion of 1-butene approached an asymptotic value of 82% with increasing Zr loadings in ZrSi. The gas-phase products were *cis*- and *trans*-2-butene isomers in equilibrium amounts, and trace amounts of isobutene, propene, pentenes, and butanes (3% selectivity from 1-butene). Under the reaction conditions used, the double-bond isomerization is a much more facile reaction than skeletal isomerization and side-reactions.[58] With the low conversion to isobutene and side-products, it was reasonable to calculate the equilibrium conversion of 82% based on double-bond isomerization prod-

(54) Aguayo, A. T.; Arandes, J. M.; Olazar, M.; Bilbao, J. *Ind. Eng. Chem. Res.* **1990**, *29*, 1172.

(55) Liu, Z.; Tabora, J.; Davis, R. J. *J. Catal.* **1994**, *149*, 117.

(56) Mastikhin, V. M.; Nosov, A. V.; Terskikh, V. V.; Zamaraev, K. I.; Wachs, I. E. *J. Phys. Chem.* **1994**, *98*, 13621.

(57) Bergna, H. E. In *The Colloid Chemistry of Silica,* Advances in Chemistry Series, Vol. 234; Bergna, H. E., Ed.; American Chemical Society: Washington, DC, 1994; p 1.

(58) Butler, A. C.; Nicolaides, C. P. *Catal. Today* **1993**, *18*, 443. (b) Houzvicka, J.; Ponec, V. *Catal. Rev.-Sci. Eng.* **1997**, *39*, 319.

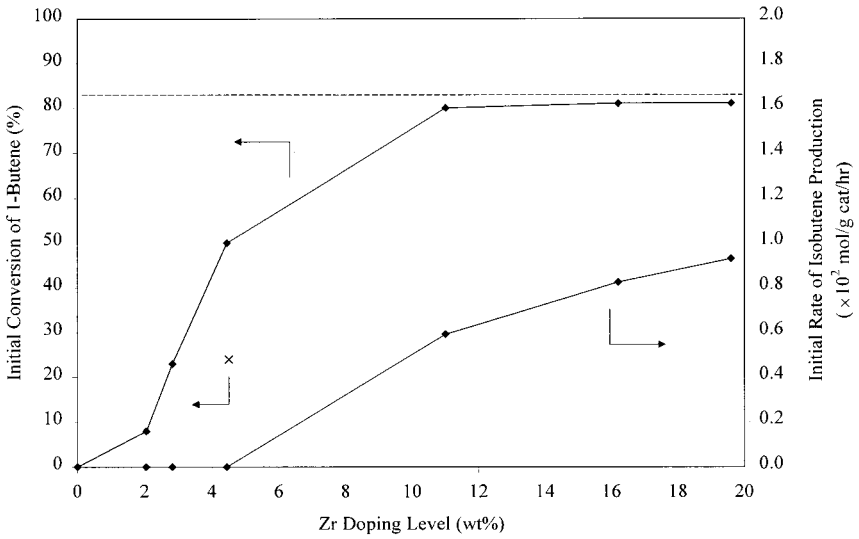

Figure 12. Initial conversion of 1-butene and initial rate of isobutene production at 350 °C as a function of Zr content in ZrSi materials prepared with $Zr(SO_4)_2$ (◆) and with $ZrOCl_2$ (×). The dotted line indicates the thermodynamic conversion of 1-butene at 350 °C (82%).

ucts. Higher conversion of 1-butene cannot occur through double-bond isomerization but may be achieved by increasing reaction rates to side-products.

The gas-phase products formed over ZrSi doped with < 5 wt % Zr were *cis*- and *trans*-2-butenes exclusively, indicating the presence of medium-strength acid sites. The more heavily doped ZrSi materials catalyzed the formation of 2-butenes and also of isobutene (Figure 12). The formation of isobutene has been studied extensively over a variety of catalysts, such as zeolites,[59] halogenated aluminas,[60] and tungsten oxide-based materials[61] because of the commercial importance of isobutene.[58] Zeolites have been proposed to catalyze skeletal isomerization via a monomolecular mechanism, i.e., a linear butene molecule rearranges into isobutene through a methylcyclopropyl carbenium ion.[59] Nonzeolitic materials have been found to catalyze a bimolecular mechanism, i.e., two butenes dimerize into an octene, which isomerizes and cracks to give isobutene.[58] Over both zeolitic and nonzeolitic catalysts, byproduct formation goes through a bimolecular pathway.

The ZrSi catalysts likely involved a bimolecular mechanism for several reasons. The monomolecular reaction pathway appears to occur only in the highly constrained micropores of zeolites, e.g., ferrierite (a 10-member ring zeolite with pore sizes of 4.2 × 5.4 Å),[58,59] which are smaller than the micropores of ZrSi2 materials. Further, the propene and pentene byproducts (roughly the same molar amounts) detected over ZrSi would have resulted from a bimolecular reaction, in which the octene intermediate cracks at a different carbon site to give disproportionation products. Small amounts of *n*-butane and isobutane were also found, resulting from hydrogen-transfer reactions.

The catalytic activity of ZrSi2-10 was examined and compared to that of SZ. Both were found very active for overall 1-butene conversion and isobutene production, but a closer examination of the product distribution revealed differences in catalytic activity (Table 7). The initial isobutene yield was higher over SZ than over ZrSi2-10 because the latter catalyst underwent greater coke formation. After 42 min on stream, both isobutene yield and selectivity decreased to similar values over both catalysts. For comparison, one of the most effective catalysts for 1-butene skeletal isomerization is ferrierite.[59] Under approximately similar 1-butene conversions and reaction conditions (350 °C, 1.4 atm and a WSHV of 2.0 h^{-1}), ferrierite was reported to have a steady-state isobutene selectivity of 81%,[59b] significantly better than the nonzeolitic ZrSi2-10 and SZ catalysts.

Gas-phase products besides butenes were detected with ZrSi2-10 and SZ, signifying that side-reactions took

Table 7. Conversion of 1-Butene over ZrSi2-10 and SZ[a]

	ZrSi2-10		SZ	
Zr content (wt %)	19.6		74	
S content (wt %)	1.33		1.61	
surface area (m^2/g)	436		94	
pore size (Å)	16		25	
product distribution (vol %)	initial	42 min TOS[d]	initial	42 min TOS[d]
methane	0.003	0.000	0.000	0.000
ethane	0.002	0.000	0.001	0.000
ethene	0.002	0.000	0.004	0.000
propane	0.008	0.000	0.003	0.000
propene	0.424	0.063	0.378	0.057
n-butane	0.094	0.001	0.040	0.009
isobutane	0.360	0.009	0.171	0.007
1-butene	0.980	2.767	1.780	2.408
trans-2-butene	1.767	4.077	3.398	4.402
cis-2-butene	1.286	3.282	2.470	3.267
isobutene	0.749	0.361	1.190	0.382
pentenes	~0.26	~0.06	~0.33	~0.05
total 1-butene conversion (%)	91	74	83	77
selectivity to isobutene (%)[b]	15.7	3.4	13.5	3.6
loss to coke formation (%)[c]	46.6	<1.0	11.1	<1.0

[a] Reaction conditions: 350 °C, 1 atm, WHSV = 5.3 h^{-1}. [b] Defined as isobutene/(total linear butenes detected). [c] Calculated as (1 − (total products detected)/(initial 1-butene)) × 100%. [d] Time on stream.

(59) Xu, W.-Q.; Yin, Y.-G.; Suib, S. L.; O'Young, C.-L. *J. Catal.* **1994**, *150*, 34. (b) Woo, H. C.; Lee, K. H.; Lee, J. S. *Appl. Catal. A: Gen.* **1996**, *134*, 147.

(60) Gayubo, A. G.; Llorens, F. J.; Cepeda, E. A.; Bilbao, J. *Ind. Eng. Chem. Res.* **1997**, *36*, 5189.

(61) Gielgens, L. H.; van Kampen, M. G. H.; Broek, M. M.; van Hardeveld, R.; Ponec, V. *J. Catal.* **1995**, *154*, 201.

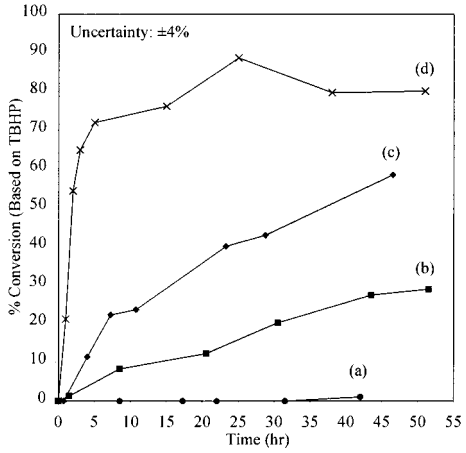

Figure 13. Conversion profiles of cis-cyclooctene epoxidation with TBHP at 40 °C over (a) ZrSi1-0, (b) ZrSi1-10, (c) ZrSi1-3C, and (d) ZrSBA-15.

place in parallel. Propene and pentenes would be produced in equal amounts from the disproportionation of butenes, as found for SZ. For ZrSi2-10, however, excess propene was detected, which could have come from the cracking of butenes, butanes, or oligomers formed during the reaction. Small amounts of methane and ethene, also likely cracking products, were detected as well. The presence of saturated hydrocarbon products indicated hydrogen-transfer reactions occurred, i.e., hydrogenation of alkenes to alkanes. These reactions are known to be catalyzed by very strong acid sites, which must be present on ZrSi2-10 and SZ. The products of these undesired reaction pathways became insignificant after 42 min, indicating the acid sites for these pathways deactivated. Also, the loss of hydrocarbons (via coke formation) became negligible. The overall conversion of 1-butene dropped to similar levels for the two catalysts. It was concluded that the very strong acid sites for the side-reactions of 1-butene deactivated from coke formation, but the moderate and strong acid sites of both catalysts for double-bond and skeletal isomerizations were still operative.

Liquid-Phase *cis*-Cyclooctene Epoxidation. ZrSi materials were tested for liquid-phase epoxidation of *cis*-cyclooctene using an organic oxidant, *tert*-butylhydroxyperoxide (TBHP). The cyclooctene oxide was the sole product. The epoxide is known to be resistant to acid-catalyzed isomerization and ring-opening reactions, making the reaction simple and convenient to follow (Figure 11b).[62] The extent of reaction was tracked by following the loss of TBHP as it reduced to *tert*-butyl alcohol. The homolytic decomposition of TBHP was found to be negligible. Pure silica ZrSi1-0 was catalytically inert, while the Zr-doped mesoporous silicas were active, indicating Zr sites were required for epoxidation to occur (Figure 13). Both ZrSi1-10 and ZrSi1-3C catalyzed the epoxidation reaction (Figure 13b−c), but ZrSi1-3C was three times more active than ZrSi1-10 with regard to turnover frequency (TOF) (Table 8). These two doped silicas have similar Zr content, surface area, and pore size, suggesting that SO_4^{2-} content was responsible for the disparity in activity. For doped

Table 8. Properties and *cis*-Cyclooctene Epoxidation Activity of Mesoporous Pure and Zr-Doped Silicas[a]

sample	Zr content (wt %)	S content (wt %)	BET SA (m^2/g)	pore size (Å)	TOF (h^{-1})[b]
ZrSi1-0	0.0	0.00	1250	25	0.00
ZrSi1-10	4.4	0.14	1066	22	0.21
ZrSi1-3C	4.5	0.00	1150	21	0.65
ZrSBA-15	4.8	0.00	942	80	5.77

[a] Reaction conditions: 40 °C, 1 atm, 4 mL of CH_2Cl_2, 7.7 mmol of *cis*-cyclooctene, 0.5 mmol of TBHP, 100 μL of chlorobenzene, 24 μmol of Zr^{4+} or 50 mg of pure silica ZrSi1-0. [b] Based on the first 3 h.

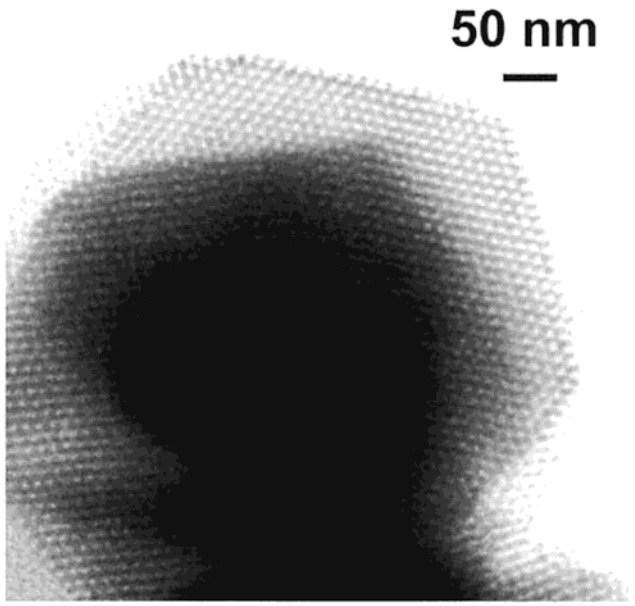

Figure 14. TEM image of ZrSBA-15, after calcination at 540 °C.

zeolites used as redox catalysts, an important requirement was the presence of coordinatively unsaturated metal cations as strong Lewis acid sites (and as weak redox sites so that the undesired decomposition of the oxidizing agent would not be promoted).[63] While ZrSi1-10 and ZrSi1-3C possessed surface-exposed Zr sites, some of the Zr cations in ZrSi1-10 were inferred to be coordinated with surface sulfate groups. These sulfates reduced the amount of active Zr sites available for epoxidation catalysis, as substantiated by the difference in epoxidation rates between ZrSi1-10 and ZrSi1-3C.

The effect of pore size on epoxidation was examined. An ultralarge-pore analogue of ZrSi was prepared in the form of Zr-doped SBA-15 (Figure 14). Its pore size was 80 Å, about 4 times larger than that of ZrSi1-3C (Table 8). The overall TBHP conversion stabilized at ~80% over ZrSBA-15 (Figure 13d) but was still increasing over ZrSi1-3C (~55%). The TOF of this ultralarge-pore material was about 9 times greater than the TOF of ZrSi1-3C.

The enhancement in reaction rate of ZrSBA-15 could be explained in terms of pore size and its effect on the diffusion of reactants. Diffusion in liquids is characterized by diffusion coefficient values on the order of 10^{-5} cm^2/s, as compared to bulk gas-phase diffusivities of 10^{-1} cm^2/s.[64] Gas-phase diffusion in a porous matrix becomes affected by pore sizes below 100 nm, where

(62) Rudolph, J.; Reddy, K. L.; Chiang, J. P.; Sharpless, K. B. *J. Am. Chem. Soc.* **1997**, *119*, 6189.

(63) Sheldon, R. A.; Wallau, M.; Arends, I. W. C. E.; Schuchardt, U. *Acc. Chem. Res.* **1998**, *31*, 485.

Knudsen diffusion occurs. When the pore size approaches the mean free path of gas molecules, as in the case of Knudsen diffusion, the kinetic theory of gases gives $D_K = 9700R\sqrt{(T/M)}$, where D_K is Knudsen diffusivity (cm^2/s), R is pore radius (cm), T is absolute temperature, and M is molecular weight.[65] Smaller pores lead to reduced gas diffusion, and a similar effect on diffusion through a liquid in fine pores could be expected. The 21-Å pores would hinder diffusive transport of TBHP (5.1 Å) and *cis*-cyclooctene (5.3 Å) more than the 80-Å pores, resulting in a lower effective diffusivity D_{eff} in ZrSil-3C as compared to ZrSBA-15. At high Thiele moduli conditions where strong pore diffusion effects occur, the effectiveness factor is roughly proportional to D_{eff}, and therefore the overall epoxidation reaction rate would be lowered for ZrSil-3C relative to ZrSBA-15.

ZrSBA-15 had a smaller surface area than ZrSi1-3C and might be expected to reduce rate of epoxidation. Its higher TOF indicated that accessibility to the active sites significantly facilitated the epoxidation reaction. It was noted that other factors could also have an effect on the observed catalytic behavior, such as nonuniform particle size, bent pore channels, channels of varying lengths, and differences in surface Zr enrichment (Table 6).

(64) Satterfield, C. N. *Heterogeneous Catalysis in Industrial Practice*, 2nd ed.; McGraw-Hill: New York, 1991.

(65) Satterfield, C. N. *Mass Transfer in Heterogeneous Catalysis*; Krieger Publishing: New York, 1981.

Conclusions

Thermally stable, well-defined porous silicas containing up to 20 wt % Zr dopants were successfully synthesized. The low-pH condition was critical toward achieving such high levels of Zr doping while maintaining the MCM-41-type mesostructure. The incorporation of Zr was found highly dependent on the synthesis pH and the nature of the Zr salt precursor. The resulting ZrSi mesoporous materials had very high surface areas, uniform pore sizes, and pore ordering, with the quality of the porous structure dependent on Zr content. Microporosity was achieved when > 10 wt % Zr was incorporated into the silica-based framework. Zr cations were found highly dispersed and no bulk zirconia phases were detected. The ZrSi materials showed high activity in the gas-phase isomerization of 1-butene, which increased with the Zr doping level and the surface sulfate content. ZrSi with ∼20 wt % Zr content exhibited skeletal isomerization activity comparable to sulfated zirconia. ZrSi also exhibited activity for the liquid-phase *cis*-cyclooctene epoxidation, with the reaction rate significantly bolstered by ultralarge pores.

Acknowledgment. This work was supported by the Camille and Henry Dreyfus Foundation. The authors acknowledge E. S. Jeng for assistance in the preparation of ZrSi materials, and C.-C. Wang for assistance with the UV−Vis experiments.

CM010076+